DNA-TR-87-144

TWO-METER LASER MATERIAL RESPONSE IMPULSE MEASUREMENTS

K. Robertson
M. C. Cates
Maxwell Laboratories, Inc.
8888 Balboa Avenue
San Diego, CA 92123-1577

11 February 1988

Technical Report

CONTRACT No. DNA 001-85-C-0186

Approved for public release;
distribution is unlimited.

THIS WORK WAS SPONSORED BY THE DEFENSE NUCLEAR AGENCY UNDER RDT&E RMC CODES B3420854664 XC 00021 25904D, B3420854664 X B 00009 25904D, B3420854664 X B 00008 25904D AND B3420854662 A X 00021 25904D.

Prepared for
Director
Defense Nuclear Agency
Washington, DC 20305-1000

Destroy this report when it is no longer needed. Do not return to sender.

PLEASE NOTIFY THE DEFENSE NUCLEAR AGENCY, ATTN: CSTI, WASHINGTON, DC 20305-1000, IF YOUR ADDRESS IS INCORRECT, IF YOU WISH IT DELETED FROM THE DISTRIBUTION LIST, OR IF THE ADDRESSEE IS NO LONGER EMPLOYED BY YOUR ORGANIZATION.

DISTRIBUTION LIST UPDATE

This mailer is provided to enable DNA to maintain current distribution lists for reports. We would appreciate your providing the requested information.

- ☐ Add the individual listed to your distribution list.
- ☐ Delete the cited organization/individual.
- ☐ Change of address.

NAME: _____

ORGANIZATION: _____

OLD ADDRESS	CURRENT ADDRESS
_____	_____
_____	_____
_____	_____

TELEPHONE NUMBER: (___) _____

SUBJECT AREA(s) OF INTEREST:

_____	_____
_____	_____
_____	_____

DNA OR OTHER GOVERNMENT CONTRACT NUMBER: _____

CERTIFICATION OF NEED-TO-KNOW BY GOVERNMENT SPONSOR (if other than DNA):

SPONSORING ORGANIZATION: _____

CONTRACTING OFFICER OR REPRESENTATIVE: _____

SIGNATURE: _____

CUT HERE AND RETURN

Director
Defense Nuclear Agency
ATTN: TITL
Washington, DC 20305-1000

Director
Defense Nuclear Agency
ATTN: TITL
Washington, DC 20305-1000

REPORT DOCUMENTATION PAGE

1a REPORT SECURITY CLASSIFICATION UNCLASSIFIED	1b RESTRICTIVE MARKINGS
2a SECURITY CLASSIFICATION AUTHORITY N/A since Unclassified	3 DISTRIBUTION/AVAILABILITY OF REPORT Approved for public release; distribution is unlimited.
2b DECLASSIFICATION/DOWNGRADING SCHEDULE N/A since Unclassified	
4 PERFORMING ORGANIZATION REPORT NUMBER(S)	5 MONITORING ORGANIZATION REPORT NUMBER(S) DNA-TR-87-144
6a NAME OF PERFORMING ORGANIZATION Maxwell Laboratories, Inc. 6b OFFICE SYMBOL (if applicable)	7a NAME OF MONITORING ORGANIZATION Director Defense Nuclear Agency
6c ADDRESS (City, State, and ZIP Code) 8888 Balboa Avenue San Diego, CA 92123-1577	7b ADDRESS (City, State, and ZIP Code) Washington, DC 20305-1000
8a NAME OF FUNDING/SPONSORING ORGANIZATION 8b OFFICE SYMBOL (if applicable) SPWE/Wolf	9 PROCUREMENT INSTRUMENT IDENTIFICATION NUMBER DNA 001-85-C-0186
8c ADDRESS (City, State, and ZIP Code)	10 SOURCE OF FUNDING NUMBERS PROGRAM ELEMENT NO. 62715H; PROJECT NO. X X A; TASK NO. C B X; WORK UNIT ACCESSION NO DH008920
11 TITLE (Include Security Classification) TWO-METER LASER MATERIAL RESPONSE IMPULSE MEASUREMENTS	
12 PERSONAL AUTHOR(S) Robertson, Karin and Cates, Michael C.	
13a TYPE OF REPORT Technical 13b. TIME COVERED FROM 850419 TO 870401	14. DATE OF REPORT (Year, Month, Day) 880211 15. PAGE COUNT 44
16 SUPPLEMENTARY NOTATION This work was sponsored by the Defense Nuclear Agency under RDT&E RMC Codes B3420854664 X C 00021 25904D, B3420854664 X B 00009 25904D, B3420854664 X B 00008 25904D and B3420854662 A	

17 COSATI CODES			18. SUBJECT TERMS (Continue on reverse if necessary and identyfy by block number)
FIELD	GROUP	SUB-GROUP	Laser/Target Interaction Impulse
9	3		
20	11		

19. ABSTRACT (Continue on reverse if necessary and identify by block number)

The SDIO/MLI Two-Meter Laser was converted to KrF operation. The laser output (250 J in 1.8 us) provided kJ/cm^2 fluences on 1100-H118 aluminum targets.

The impulse delivered to the target was measured and compared with 2-D hydrocode predictions.

The results of previous MLI Impulse measurements at XeF wavelength are summarized.

20 DISTRIBUTION/AVAILABILITY OF ABSTRACT ☐ UNCLASSIFIED/UNLIMITED ☒ SAME AS REPORT ☐ DTIC USERS	21 ABSTRACT SECURITY CLASSIFICATION UNCLASSIFIED
22a NAME OF RESPONSIBLE INDIVIDUAL Dennie F. Maddox	22b TELEPHONE (Include Area Code) (202) 325-7042 22c. OFFICE SYMBOL DNA/CSTI

DD FORM 1473 84 APR edition may be used until exhausted.
All other editions are obsolete.

16. SUPPLEMENTARY NOTATION (Continued)

X 00021 25904D.

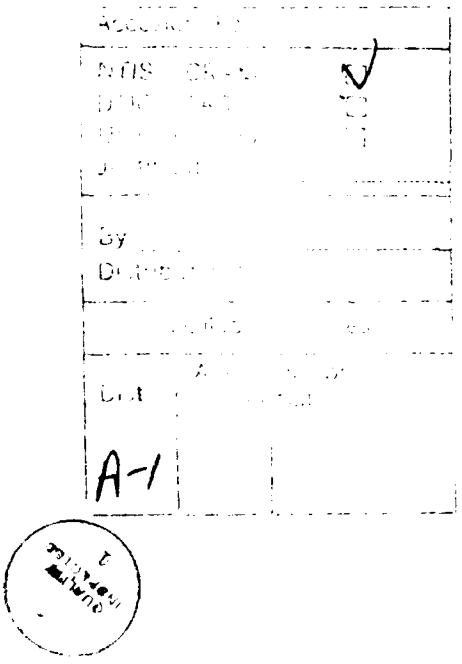

SUMMARY

Impulse generated by Excimer-Laser-target interaction has been extensively studied at Maxwell Laboratories, Inc. This report presents results of impulse measurements on aluminum targets using the SDIO/MLI Two-Meter Laser operating with KrF as the lasing media. The results of previous MLI impulse measurements using XeF laser media are summarized.

The work presented in this report was motivated by earlier impulse measurements also taken on the Two-Meter Laser under S-Cubed's Material Response Contract DNA 001-84-C-0088 (reported in Final Technical Report (Draft) SSS-R-86-7629). The data showed much higher impulse to energy ratios than predicted. Additionally, work done elsewhere gave lower I/E values than those found at MLI. The initial MLI impulse studies used a Fotonic gauge as a velocity sensor. As a check on its accuracy, impulse was measured using a simple pendulum; the results agreed with the Fotonic gauge data. A careful investigation of the pendulum experimental technique followed; no problems were found.

The S-Cubed ZOOS code was also examined. It is a 1 1/2 - D code, and only accounts for impulse delivered under the Laser footprint. Additional momentum, however, is provided outside the laser spot via the plasma cloud that results from the laser-target interaction. To investigate this, experiments were performed using a flood-loaded target. Lower I/E coefficients were measured with this target than had been measured with a partially illuminated target. The flood-loaded target data agreed with the ZOOS 1 1/2 - D code.

The Air Force Weapons Laboratories measured impulse at AVCO-Everett Research Laboratories, using a Linear Velocity Transducer as a velocity sensor. This device was brought to MLI, and a further series of impulse measurements was done. The LVT I/E coefficients measured at MLI were significantly higher than those found at AERL, but lower than those measured at MLI using the simple pendulum.

The efforts mentioned above have been described elsewhere. The AFWL/AERL work was reported in "The Interaction of High Energy Single Pulse

XeF Laser Radiation with Solid Targets", Finai Report, AFWL-TR-85-126. The MLI XeF impulse studies were reported to S-Cubed in MLR-2320. The AFWL/MLI experiments were detailed in "An Experimental Investigation of Impulse Production by a Pulsed XeF Laser", Edwards et al, AFWL-TR-86-155

Additional studies are presented here. We report the results of the most recent impulse measurements, which used the SDIO/MLI Two-Meter Laser with KrF as the lasing medium. As the Two-Meter Laser had operated exclusively with XeF for the past few years, the switch to KrF required several changes to the facility. These changes will be described. Also, results of the power/energy calibration of the calorimeters on which laser energy measurements rely are presented. A comparison of different data sets is made, and the similarities and differences (particularly the pressures at which the data were taken) are discussed.

The report will begin with a brief description of the Two-Meter Laser, followed by a discussion of the changes to the facility required for operation at 248 nm. The KrF impulse results are presented. The calorimeter calibration is described. Different impulse data sets are compared, and a summary presented.

TABLE OF CONTENTS

LIST OF ILLUSTRATIONS

LIST OF TABLES

SECTION 1
TWO-METER LASER MATERIALS RESPONSE FACILITY

1.1 INTRODUCTION.

The Two-Meter Laser Materials Response Facility consists of the SDIO/MLI Two-Meter Laser, an evacuable target chamber, a beam train to direct and focus the laser onto the target, numerous diagnostics for laser parameters (energy, pulseshape, uniformity, etc.), diagnostics for the Laser-target interaction (impulse, stress, plasma flux, etc.) and data collection equipment.

Over the past few years, the SDIO/MLI Meter laser has operated using XeF as the lasing medium.[1] [2] The change to KrF required several changes in the facility. All of the elements in the beam train were changed. The gas handling system was expanded to enable the safe use of fluorine. A different alignment laser was used, and the alignment procedure was modified. The target chamber was elongated so that the laser spot size incident on the chamber window was large enough to avoid damage. Certain diagnostic instruments were changed to accommodate the KrF 248 nm wavelength. These changes will be discussed in the following sections.

1.2 TWO-METER LASER.

The Two-Meter Laser is a large, e-beam pumped device It is pumped on one side only, and is single shot. A seven stage Marx bank capable of storing 151 kJ, with a maximum erected voltage of 840 kV powers the laser. A self breaking peaking switch, located just before the diode, sharpens the rising edge of the pulse. The carbon felt cold cathode is 20 cm X 200 cm. Current density at the cathode is 20 A/cm^2. Electron deposition into the laser chamber is enhanced by a 550 G guide field, provided by modified Helmholtz coils. Approximately 50 percent of the current is transmitted through the Hibachi structure and 3 mil aluminum foil into the laser chamber, giving a current

[1] J.R. Oldenettle, "Two Meter Upgrade", MLR-1297, November 1982.
[2] J.R. Oldenettle, F.D. Feiock and G.R. Miscikowski, "Large-Aperture Mode Formation and Laser Performance Experiments", Volume II MLR-1805, Nov. 1983.

density in the optical cavity of 10 A/cm^2. The electrical pulse length is two microseconds, and is terminated by two parallel diverter switches. Typical current and voltage traces are shown in Figure 1.

A bottom axis, positive branch confocal unstable resonator with a magnification of 1.75 forms the optical cavity. The pumped volume within the cavity is 17 X 10 X 200 cm^3. The laser mirrors are internal to the laser chamber; an uncoated 30 cm diameter, 5 cm thick UV grade synthetic fused silica window provides the pressure seal. The output beam is shaped like an inverted U, and is clipped by an aperture to 7.5 x 15 cm^2, giving a rectangular spot with a 2:1 aspect ratio.

The laser produced up to 250 J during the series of KrF experiments. However, to avoid damage to the beam train optics the marx charge voltage was lowered from 60 kV to 50 kV. This resulted in a laser output of approximately 150 J, with ~95 J on target. The lower charge voltage also caused the KrF laser pulse shape to differ from that of the XeF laser: The KrF laser "ramps up" to full power while the XeF turns on immediately. Representative pulse shapes are shown in Figure 2. The gas mix used for the KrF laser was 3.8 torr F_2, 76 torr Kr and 1440 torr of Ar. The SDIO/MLI Two-Meter Laser reliably gave up to 14 target shots per day during the experimental series.

1.3 DIAGNOSTIC ROOM CHANGES.

Major changes were made in the diagnostic room. The layout is shown in Figure 3. The new beam train consists of a 23 cm dia, 2.5 m radius of curvature focusing lens, in order to followed by the 20 cm dia, 4 cm thick vacuum chamber window. Reflections from the window are used to measure pulse energy and temporal pulse shape, the latter via a second reflection off a beam splitter in front of the calorimeter. Each optical surface is canted to avoid unwanted reflections coupling into the system. All transmissive optics are made of UV grade synthetic fused silica.

The target chamber had to be lengthened so that the vacuum window could be moved closer to the focusing lens in order to reduce the optics loading

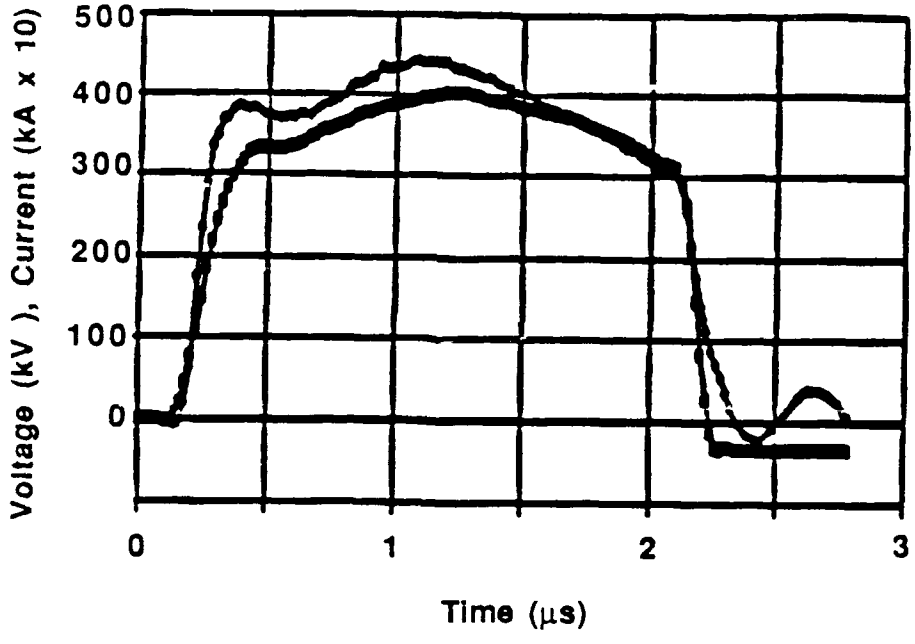

Figure 1. Gun voltage (upper curve) and transmitted current (lower curve) for 60 kV charge voltage.

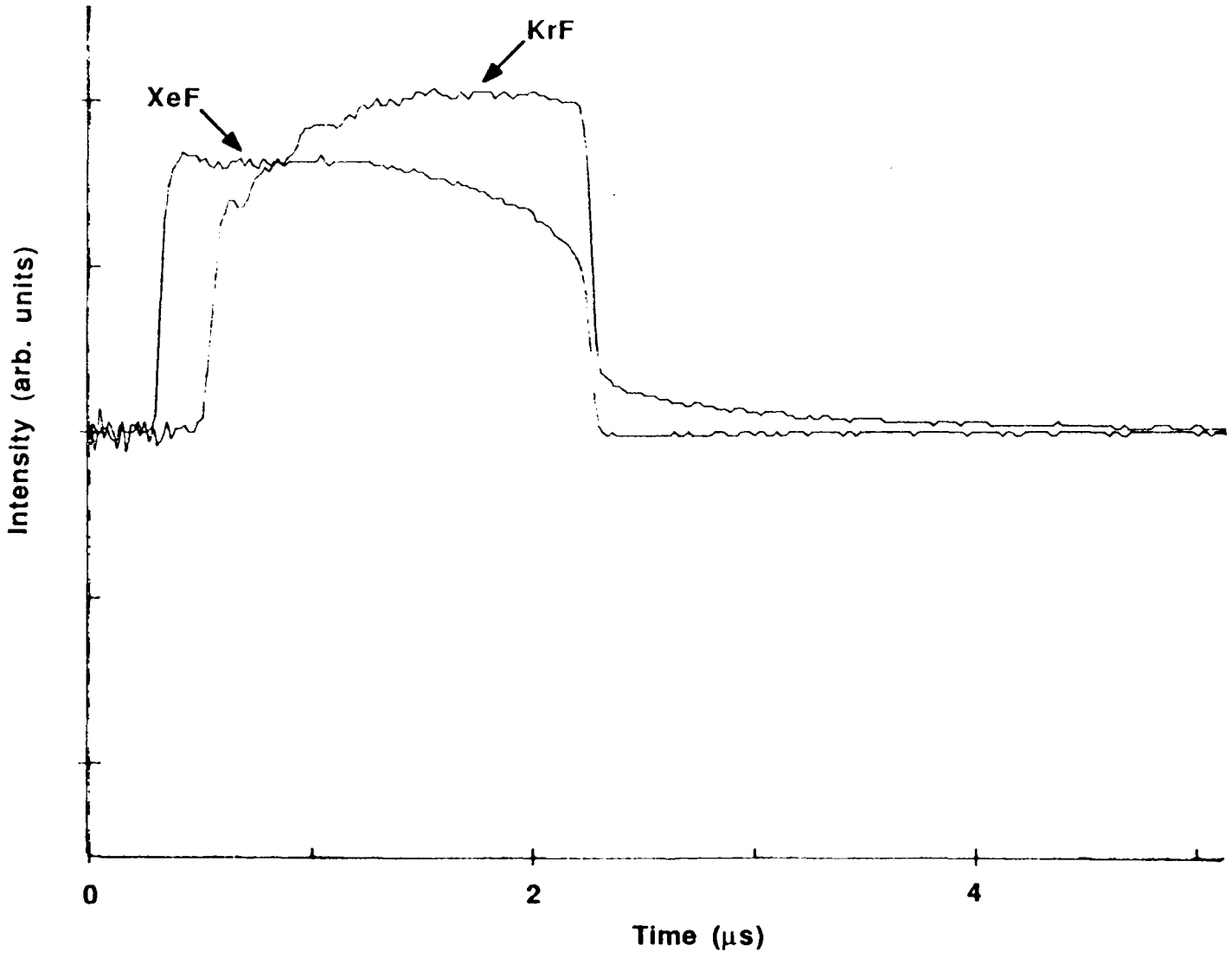

Figure 2. Laser photodiode.

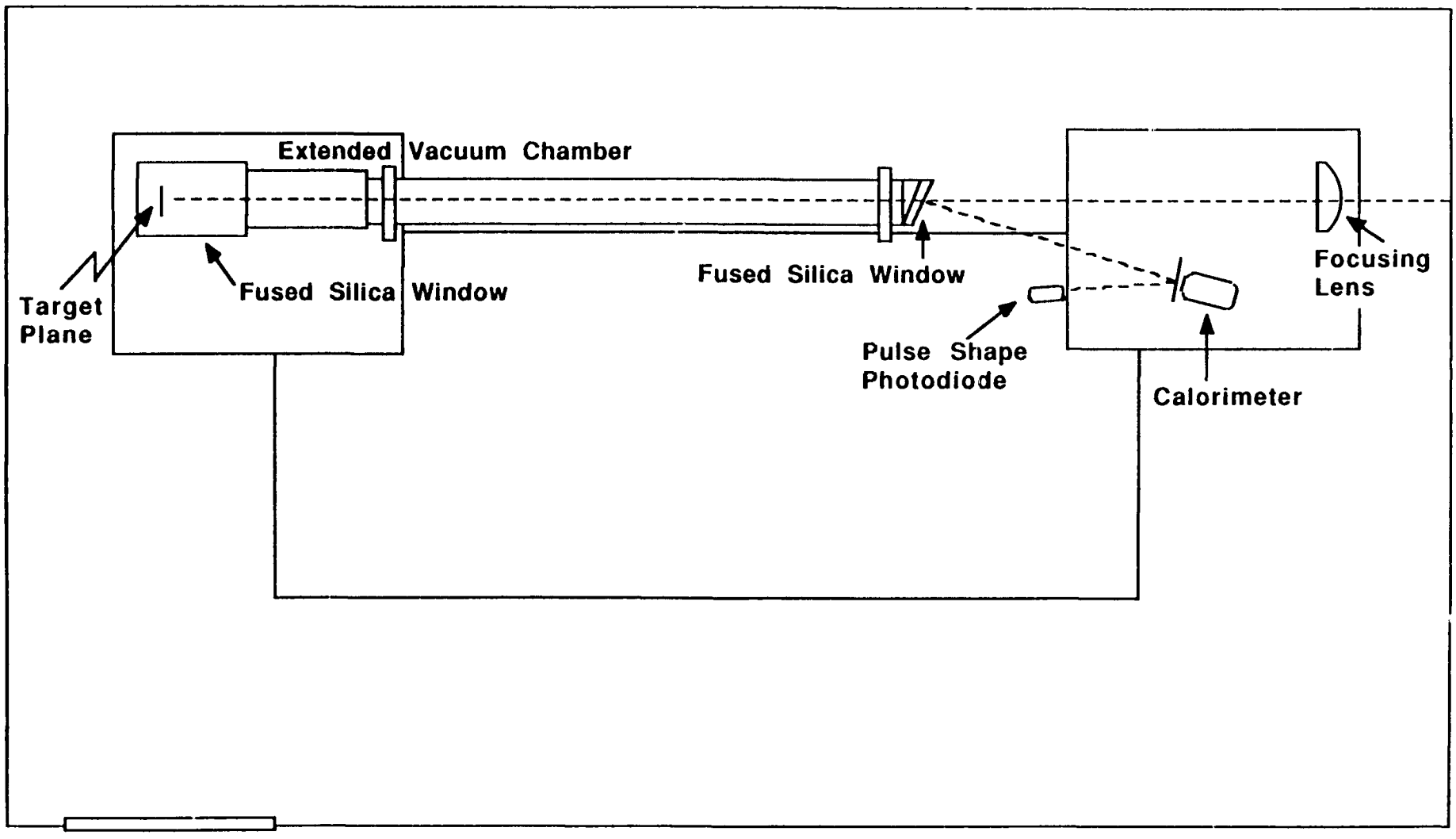

Figure 3. Diagnostic room layout.

below the damage threshold. Initial attempts to use the unmodified chamber, which had a 7.5 cm dia window, failed, as the incident fluence (approximately 11.5 J/cm^2) damaged the window. With the extension, the cross section of the laser beam on the new window is approximately 50 cm^2, and no damage to the optic is observed.

Only a few changes were made to the diagnostic system. New calorimeters (Scientech Model 38-0403) for 248 nm light were installed. A line filter (Corion G10-250-A) was placed in front of the pulse shape photodiode (Hamamatsu R110 3U-02), to ensure that we measured only laser light. The fast signals were stored on Data Precision 6000 waveform analyzers. The calorimeter data were recorded using an Omega chart recorder (Model 595). The specific diagnostic setup used on the KrF experiments will be described later.

1.4 ALIGNMENT PROCEDURE.

The 248 nm wavelength of KrF presented difficulties in aligning the laser cavity and in aiming the beam in the target room. The Ar^+ laser previously used for XeF alignment does not have a line sufficiently close to the KrF frequency, so it was replaced by a Questek Model 2240 excimer laser. A new alignment beam train was required, as the optics in the former were unsuitable for 248 nm.

The alignment beam is clipped by an aperture, giving a 1 mm dia pencil of light. This is used to define the optical axis, and acts as the core of the laser for alignment purposes. When the resonator is aligned, the alignment output is collimated and the same size as the laser output. The light is then aimed at the target by moving the focusing lens, and diagnostic instruments are easily moved into position.

Fluorine, however, absorbs at 248 nm, reducing the intensity of the light in the target room. If a mixture which includes fluorine is in the laser cavity, the pattern that results at the target plane is not a 2:1 rectangle; rather it is a set of dim, stacked, slightly overlapping rectangles. The observed pattern was modeled (using ray optics) by assuming that the alignment beam is slightly

divergent. The light passes through the resonator and beam train to the target plane and forms a stacked box pattern. Each box consists of light that has made the same number of round trips through the resonator, due to the unstable resonator's property of demagnifying the divergence with successive round trips. The model generated target plane pattern is shown in Figure 4, and agrees with the pattern observed in alignment attempts. The result is that it is virtually impossible to align the system with a mixture including fluorine in the laser chamber. Therefore, the laser was filled with krypton and argon to 1 atm, aligned and then the remainder of the gas was added. This alignment procedure worked well.

1.5 GAS HANDLING SYSTEM.

Fluorine is a dangerous and extremely reactive gas. While the hazards associated with fluorine use were lessened by employing a 5% F_2, 95% Ar mixture, special precautions were still taken. For laboratory safety, the fluorine itself was stored outside, in a shelter that protected it from the weather. The gas was passed through a HF trap (Matheson 68-1008) to prevent HF from reaching the laser chamber and etching the optics. A single, 0.6 cm stainless steel line ran into the laboratory to the gas handling station. The gas handling station itself did not require modification. The laser chamber venting system was changed so that it could be remotely operated, and an halogen filter (Applied Photonics Model DHF-100) was added, so that fluorine was not vented to the atmosphere. These changes in the gas handling system enabled safe and uneventful use of fluorine for this series of experiments.

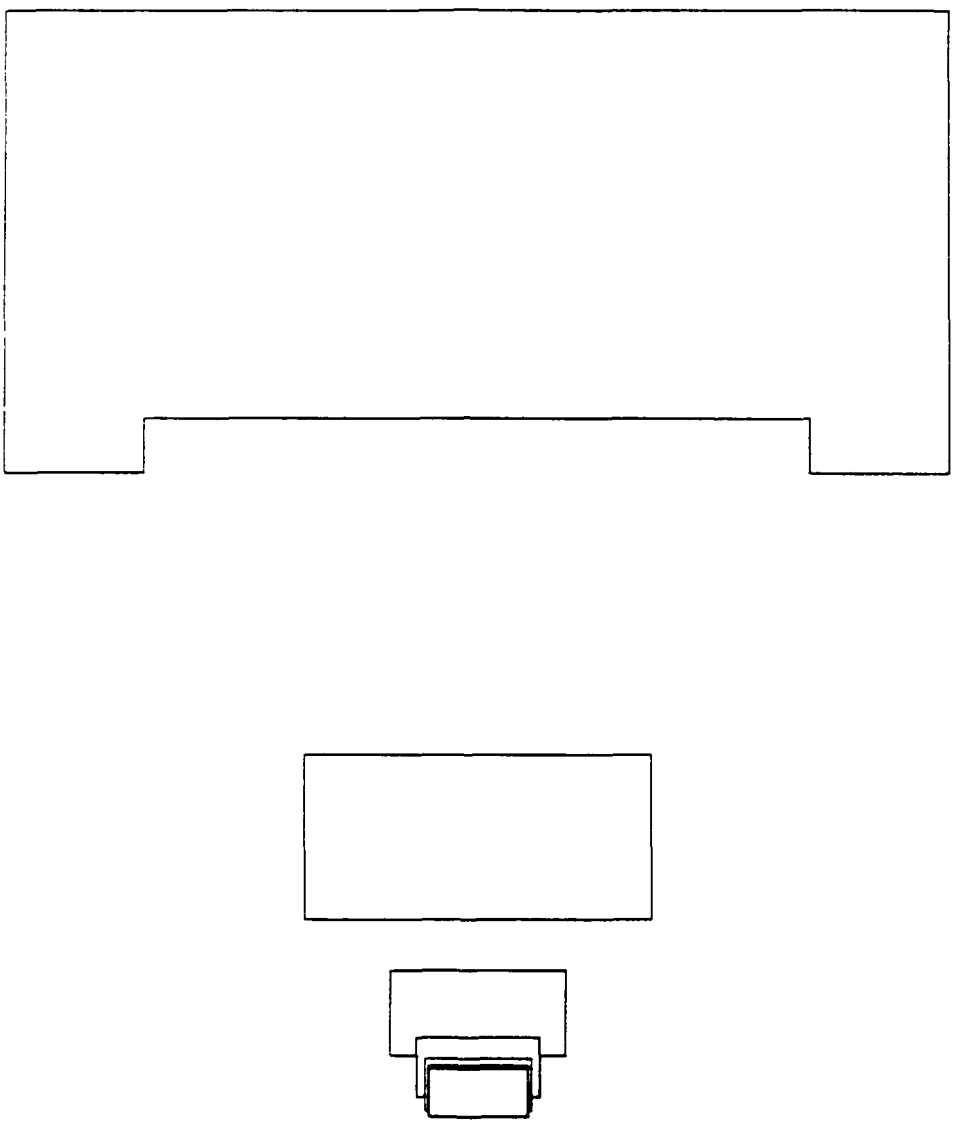

Figure 4. Pattern at target plane.

SECTION 2
KrF LASER IMPULSE MEASUREMENTS

2.1 INTRODUCTION.

The impulse delivered to the target is due to a combination of the following effects: material directly under the laser spot ablating, re-radiation of the plasma plume causing mass removal outside the laser spot, and the expansion of the high-pressure plasma "bubble" beyond the laser spot to provide a late-time impulse. The 2-dimensional STREAK code was used to predict the magnitude of these effects for a KrF laser with a fluence of 1000 J/cm^2: The ablation of material directly under the laser spot accounts for approximately 80% of the total impulse. The remaining 20% is due to the plasma expansion, with re-radiation having a negligible effect.[3]

2.2 TARGET DESCRIPTION.

The target is a 0.6 cm dia disk of 25 mm aluminum; the alloy is 1100-H118. The target is glued to a pendulum mounted on a rigid "T" hanger. The bob is a cylinder 2 cm in diameter by 1.3 cm thick. The bob center, which is also the impact point, hangs 5.8 cm below the axis of rotation. The pendulum size is chosen so that the plasma expansion effects will be measured and the mass of the material vaporized is small in comparison to the mass of the target; the bob weighs 10.8g, the hanger 2.1g.

2.3 IMPULSE MEASUREMENT.

The total momentum is found by measuring the velocity of the target after it has been struck by the laser. Experiments are performed at approximately 200 millitorr. The velocity of the target is measured by occluding a He-Ne beam which passes directly behind the target. The experimental set up is shown in Figure 5. The He-Ne beam travels vertically just behind the pendulum, first passing through three 0.25 mm wires spaced approximately 0.15 mm apart that are mounted on a prism. Thus, as the pendulum passes through the beam,

[3] G. Gurtman, et al, "Response of Aluminum to Excimer Laser Irradiation", to be presented at AIAA/DNA Laser Effects and Target Response Meeting, Monteray, CA, March 15-19, 1988.

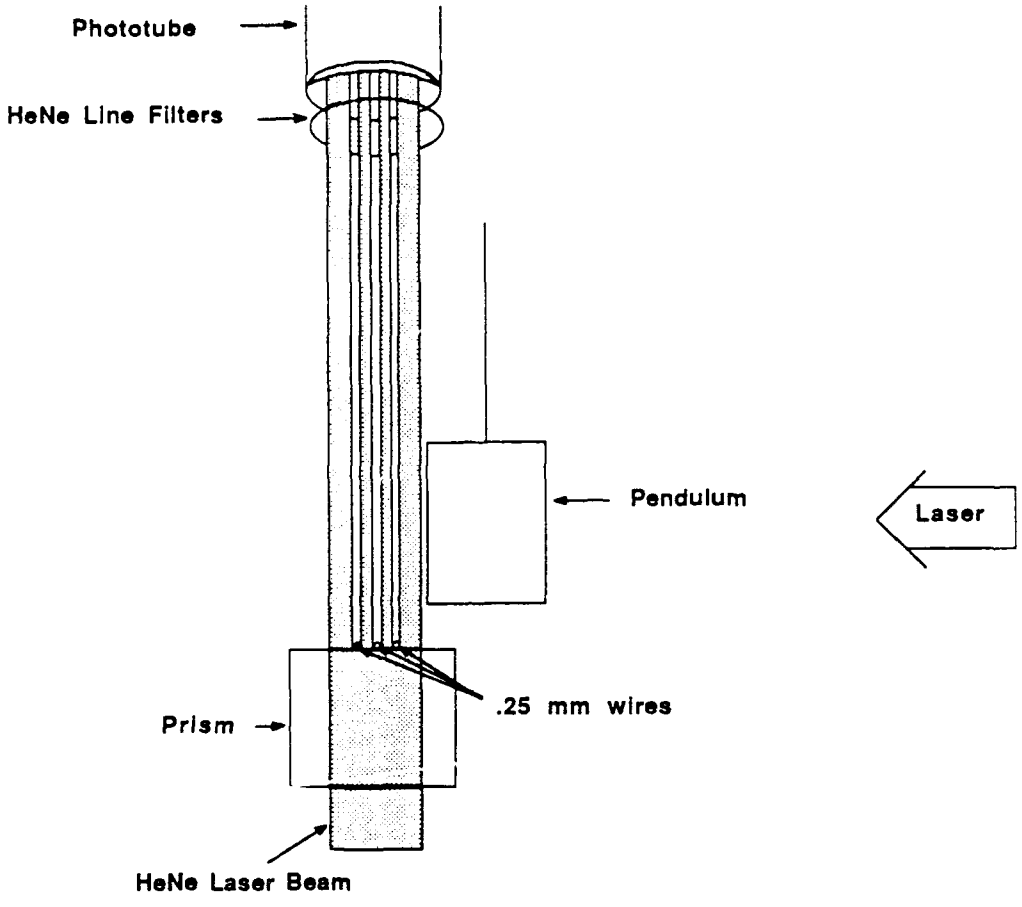

Figure 5. KrF impulse experimental set-up.

its position is marked in three spots. As the distance between the wires is known, the time that it takes to travel this distance can be measured, and the velocity calculated. Equipment used to collect the signal included a He-Ne line filter, a biplanar phototube (Hamamatsu R1103U-02) and an oscilloscope (Tektronix 7704 A). A tracing of a typical output is shown in Figure 6. The system was calibrated by releasing the pendulum from a known height, measuring the resultant velocity, and comparing it with the calculated $v=\sqrt{2gh}$ (derived from $1/2\ mv^2=mgh$). The measured velocity differed from the calculated velocity by 6 percent, which is within the error range for the measuring system.

As can be seen from the geometry of the experiment, what is measured is the velocity of the lowest point on the pendulum, while what we want to measure is the impulse delivered to the target. For constrained rotation $L=I\Delta\omega$ where L is the rotational impulse, I is the moment of inertia about the axis of rotation and ω (=v/r) is the angular velocity. Further, L = Pb, where P is the applied impulse and b is the distance from the axis of rotation to the point of impact. Therefore, $P = \frac{Iv}{br}$

For the geometrics and masses used in this set of experiments P=9.63X(velocity measured).

The energy was measured using the reflection from the chamber window, which is tilted five degrees with respect to the incoming beam. This light passes through a beam splitter, and into a 10 cm (Scientech Model 38-0403) volume absorbing calorimeter. The beam splitter is at a fifteen degree angle to the incoming light, and is used both to illuminate a time history photodiode and to prevent any air currents from reaching the calorimeter absorber. The energy that reached the calorimeter is 7.86 percent of the energy on target. The beam size on the calorimeter absorber is 20 cm^2.

2.4 RESULTS.

The KrF Impulse data is summarized in Table 1 and plotted in Figure 7. The STREAK-calculated value is also shown; The agreement is seen to be excellent. The error bars shown in the figure are determined in the usual

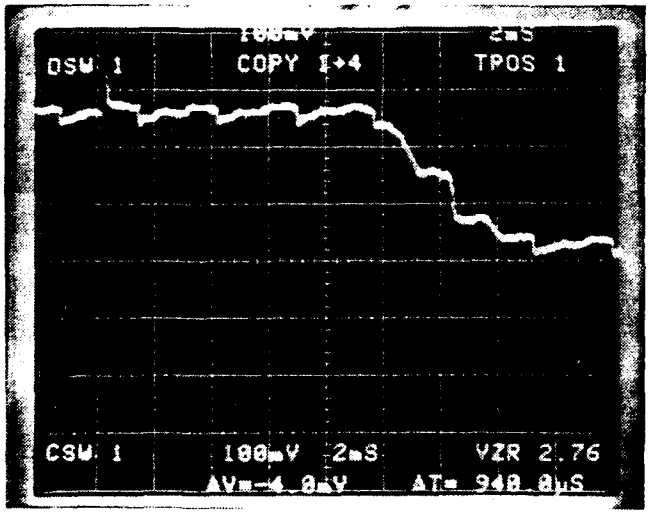

Figure 6. Oscilloscope trace of velocity measurement.

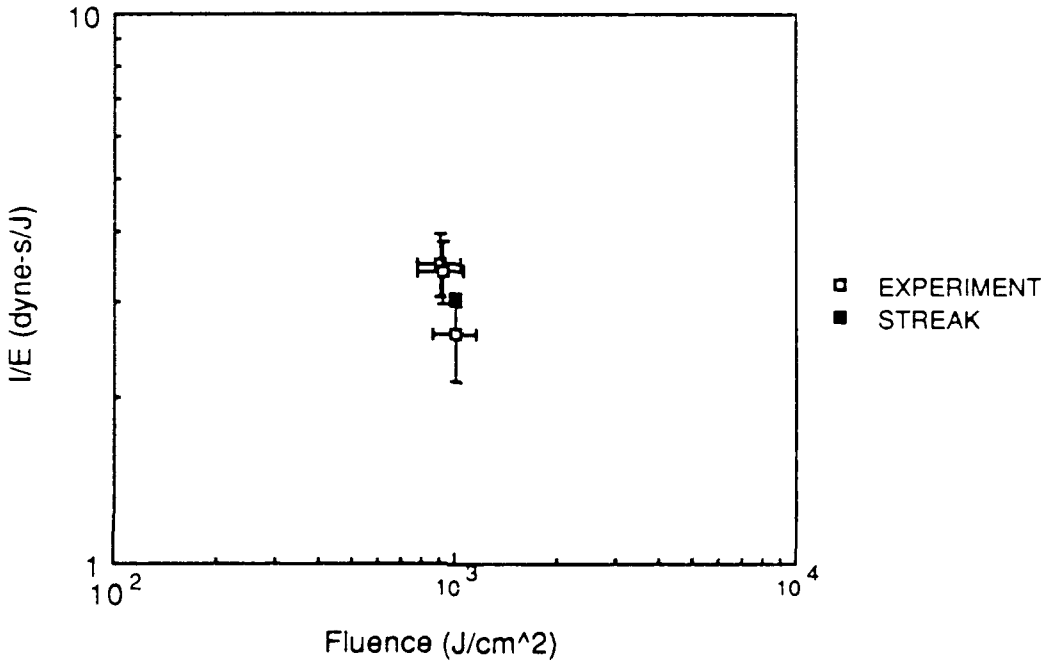

Figure 7. KrF I/E versus E/A.

manner from the individual uncertainties in the laser energy, spot size, wire spacing, and phototube voltages.

Table 1. Impulse-fluence coupling for aluminum in vacuum, KrF.

Shot Number	I/E (dyne-s/J)	E/A (J/cm^2)	Impulse (dyne-s)	Energy (J)
3	2.6	1004	264.8	102
4	3.4	915	318.4	93
5	3.5	902	318.4	91

SECTION 3
CALORIMETRY

3.1 INTRODUCTION.

As MLI's measured I/E ratios are high in comparison with other impulse studies, the accuracy of the energy measurement is of concern. Clearly, if the energy data were incorrectly interpreted to be low, I/E ratios would be incorrectly high.

There are several issues that need to be addressed in evaluating energy measurements with a volume absorbing calorimeter. First, the calorimeter measures power, but single shot energy is the quantity of interest. Second, the size and location of the incident beam may affect the accuracy of the measurement. Third, the interpretation of the calorimeter ouput signal is in doubt: should the voltage extrapolated to time = 0 or the peak voltage be taken as a measure of the laser energy? In order to address these issues and ensure the reliability of the data, an investigation of the calorimetry was undertaken.

3.2 CALORIMETER OPERATION.

Energy measurements in all Two-Meter Laser experiments use the Scientech volume absorbing calorimeter. A brief description of its operation is given here; a detailed description is found in the Scientech manual. The calorimeter is composed of an array of thermopiles connected in series, and placed between a light absorbing glass plate and a heat sink. Absorption of the laser beam produces heat, which flows through the thermopiles. This heat flow generates a thermoelectric potential, and is proportional to laser power. The signal is recorded on an Omega chart recorder. The chart recorder and calorimeter are checked regularly; the instruments reliably stay in calibration.

The Scientec Calorimeter is designed to measure power, yet here it is used to measure energy. Scientec provides a power calibration factor (mV/W) and a time constant (s), which may be divided to yield an energy calibration factor (mV/J). The power calibration factor and time constant were checked and found to agree with the factory specifications (within 2%). In order to check the

accuracy of the energy calibration factor, and the assumption that the calorimeter can be used to measure energy, a photodiode calibrated for power and energy was compared with the calorimeter output. This also resolved the issue of signal interpretation: is the voltage extrapolated to time=0 or the peak voltage the correct measure of energy? Figure 8 presents a typical calorimeter output signal.

It is possible that the size and location of the laser beam on the calorimeter can affect the accuracy of the power (or energy) measurement. The calorimeter consists of a number of theromopiles which do not fill the area behind the absorbing volume, so that a small beam could miss the thermopiles entirely, causing the thermoelectric potential to arise from radial rather than axial heat flow. The would result in a lower measured energy. Scientic specifies that the laser beam must be $\geq 25\%$ of the calorimeter surface area, and although we were operating well above this limit, a careful study of spot size and placement effects was performed for completeness.

3.3 EXPERIMENTAL METHOD.

The experimental layout is shown in Figure 9. A Questek excimer laser (model 2240) operating at 308 nm provided the laser source. The output energy was locked at 70 mJ, and the repetition rate was 50 Hz. The pulse width is approximately 10 ns. The laser is specified for 90 percent of the pulses to be within 3 percent of the lock point value. The beam was turned through 45 degrees, clipped by a 1 cm dia aperture and passed through a negative lens (used to vary the spot size) and a beam solitter into the calorimeter. The signal from the calorimeter was recorded on an Omega chart recorder. The reflection from the beam splitter bounced off a diffuser and into a photodiode (Hamamatsu R110 3U-02), through a line filter (Corion P10-310-F). The photodiode signal went to a Data Precision 6000 waveform analyzer, which collects data at 100 MHz. A train of pulses was counted and averaged. The averaged pulse was then integrated to provide the energy per pulse. In successive runs, no significant differences were found between the average energy per pulse of a thousand sample pulse train, and that of 33 pulses. This indicated that the laser output was stable and the Data Precision 6000 sampling rate was sufficient for these measurements. This set up enabled us to perform an energy calibration,

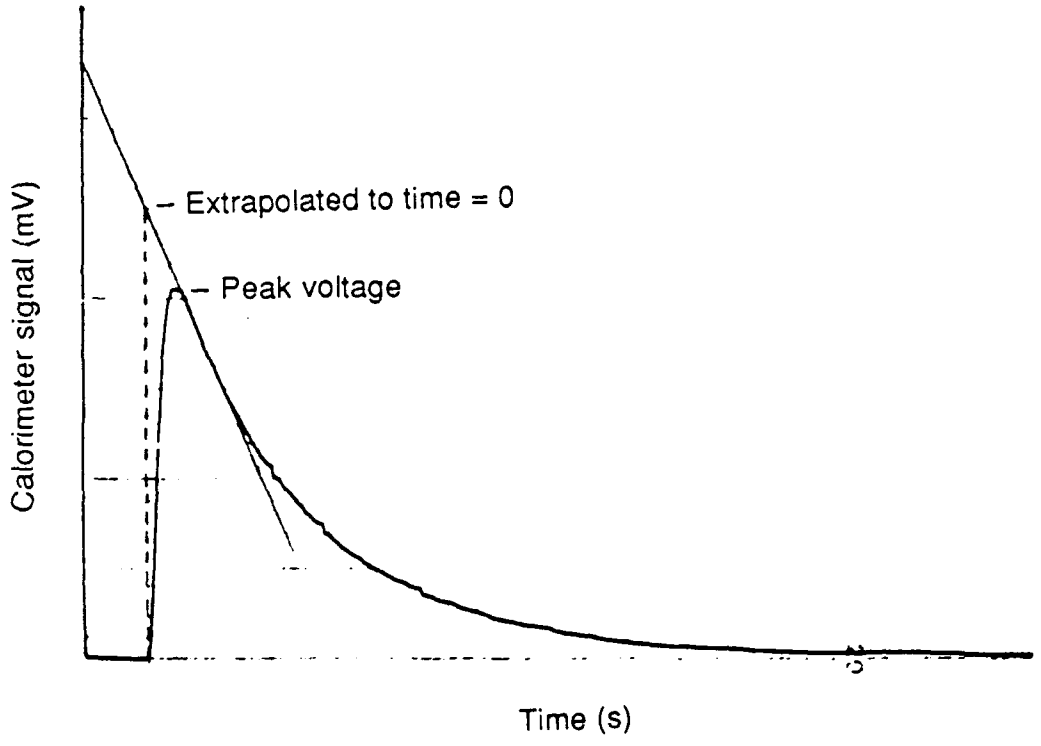

Figure 8. Typical chart recorder trace of calorimeter signal.

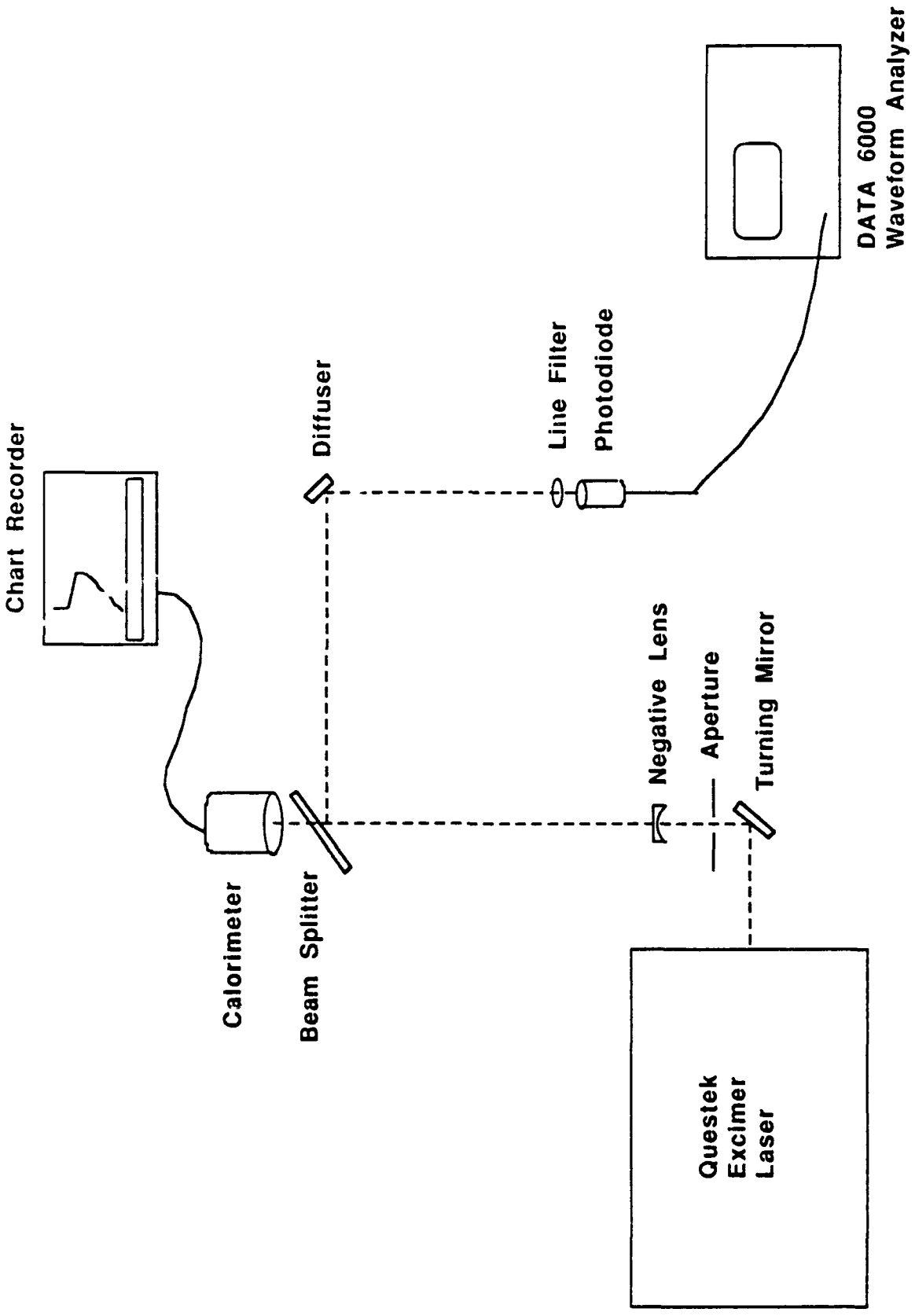

Figure 9. Calorimeter calibration set-up.

and to measure spot size and placement effects.

The energy calibration was done as follows. The Questek laser was operated at 50 Hz, 70 mJ per pulse until the calorimeter reached its steady state signal level. The mV/W conversion factor given by Scientech gave the power input into the calorimeter. The pulses into the photodiode were averaged and integrated, giving the average energy per pulse. The average power into the photodiode equals the energy per pulse multiplied by the repetition rate, as can be seen from the following:

$$\text{power} = \frac{\text{total energy}}{\text{total time}}$$

$$= \frac{(\text{energy per pulse})(\text{number of pulses})}{\frac{\text{number of pulses}}{\text{repetition rate}}}$$

$$= (\text{energy per pulse})(\text{repetition rate}) \qquad (1)$$

Thus a power calibration of the photodiode with respect to the calorimeter was made. The laser was then operated at the same repetition rate and energy, but only for a fraction of a calorimeter time constant. The photodiode signal provided both the average energy per pulse and the number of pulses, and therefore the total energy. The calibration ratio of $\text{power}_{cal}/\text{power}_{p.d.}$ was multiplied by the photodiode energy to obtain the calorimeter energy. Both a 10 cm dia (Scientech Model 38-0405, Serial Number 108) and a 20 cm dia (Scientech Model 38-0805, Serial Number 102) calorimeter were calibrated. Different spot sizes were used. The data are shown in Table 2, and are graphed in Figure 10 and 11.

The 10 cm calorimeter data clearly indicate that the most accurate energy measurement is made by using the extrapolation method. It is only when the spot is very small and off center (spot area = 1.6 percent of the absorbing area, located 2 cm from edge of calorimeter surface) that the value found this way varies significantly from that of the calibration. The result

Table 2. Calorimeter Calibration Data

Shot Number	Description	Calibration Energy	Energy - Top	Energy - Exp.
111904	10 cm - 75%	3.44 J	2.78 J	3.44 J
111905	10 cm - 75%	3.38 J	2.71 J	3.24 J
112003	10 cm - 25%	2.09 J	1.65 J	1.98 J
112004	10 cm - 25%	2.72 J	2.25 J	2.71 J
112005	10 cm - 25%	2.77 J	2.18 J	2.65 J
112008	10 cm - 1.6%	3.72 J	2.65 J	3.31 J
112011	10 cm - 1.6%	3.55 J	2.71 J	3.44 J
112012	10 cm - 1.6%	3.35 J	2.65 J	3.24 J
112013*	10 cm - 1.6%	3.47 J	2.71 J	3.31 J
112014*	10 cm - 1.6%	3.35 J	2.58 J	3.24 J
120802	20 cm - 47%	2.77 J	2.50 J	3.18 J
120803	20 cm - 47%	2.82 J	2.81 J	3.18 J
120806	20 cm - 0.2%	0.72 J	0.82 J	1.18 J
120807	20 cm - 0.2%	0.74 J	0.91 J	1.13 J
120903	20 cm - 7%	3.57 J	2.70 J	3.36 J
120904	20 cm - 7%	3.57 J	2.81 J	3.45 J
120905	20 cm - 7%	3.46 J	2.72 J	3.18 J
120906	20 cm - 0.4%	4.10 J	3.27 J	3.99 J

* Not Centered

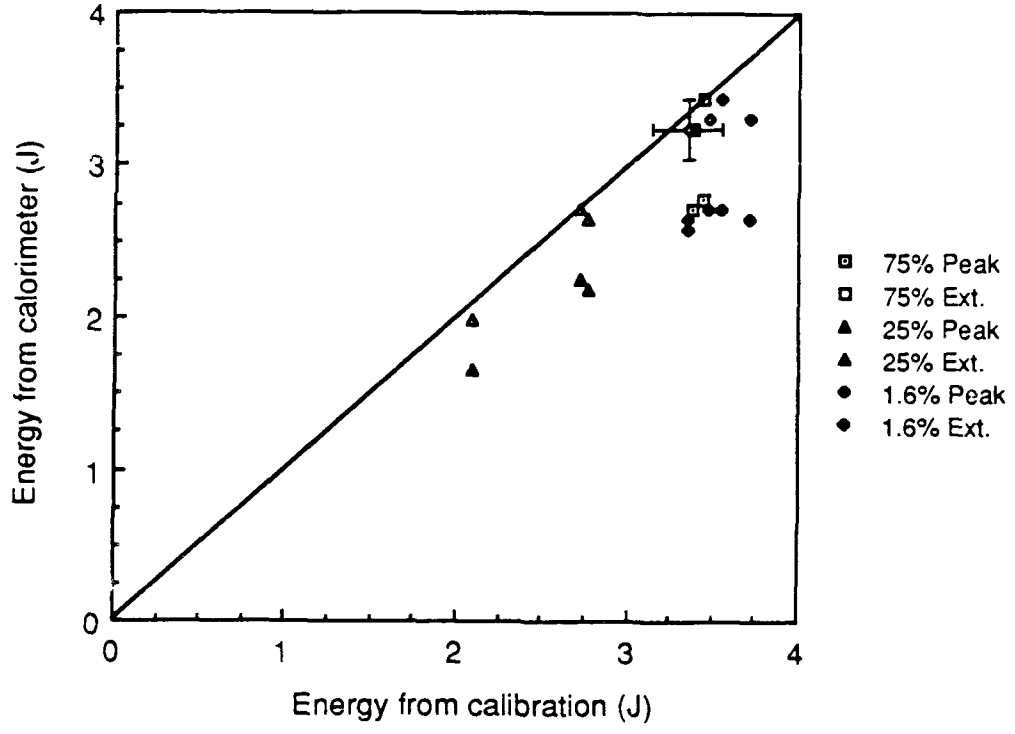

Figure 10. 10 cm diameter calorimeter calibration. Energies determined from voltage extrapolated to time = 0 and peak voltages are shown.

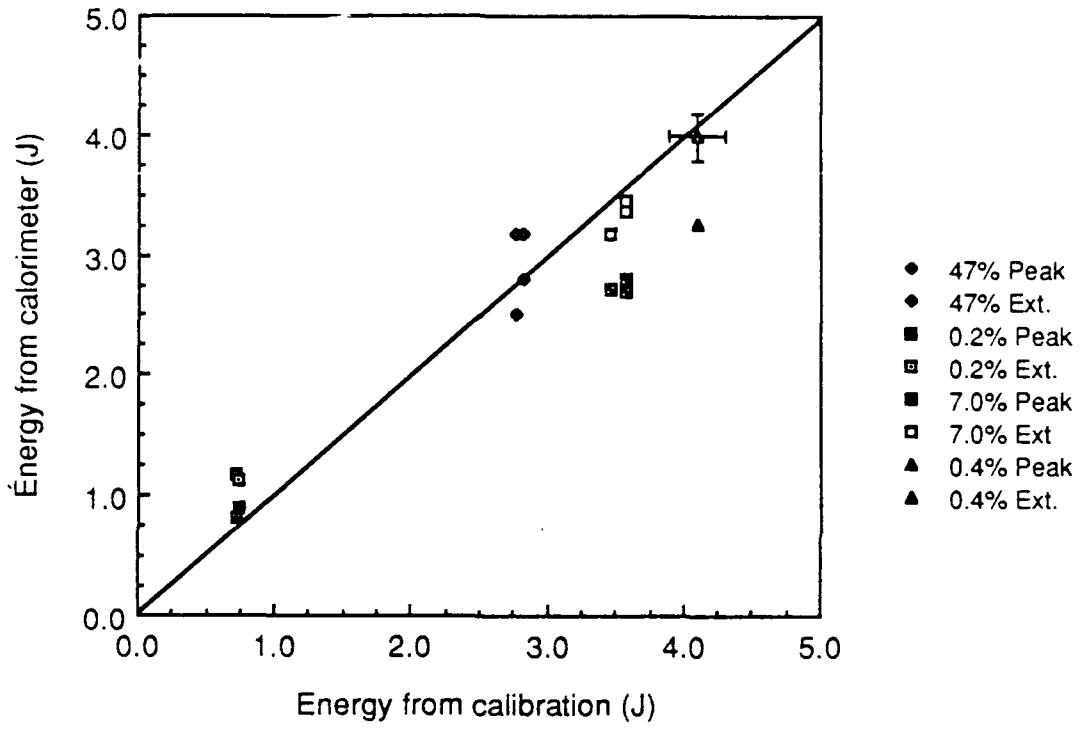

Figure 11. 20 cm diameter calorimeter calibration. Energies determined from voltage extrapolated to time = 0 and peak voltages are shown.

obtained using the peak of the signal always underestimates the energy by about 20 percent.

Although the 20 cm calibration data are not as precise as the 10 cm, the extrapolation method still provides a more accurate energy measurement than using the peak value. When the spot is very small, (area = 0.2% of absorbing surface area) neither method gives a meaningful result.

3.4 CONCLUSION.

In conclusion, the calorimeters have been calibrated as energy meters. The mV/J conversion factor was found to be appropriate, and the correct way to interpret the calorimeter signal was verified. The spot area and beam placement affected the accuracy of the measurement only at very small spot size. The spot size used in Maxwell's experiments has been at least 20 cm^2, which is 25 percent of the 10 cm calorimeter's absorbing area, and 7 percent of the 20 cm. This size is sufficient to provide an energy measurement acurate to $\pm$ 5 percent for the 10 cm calorimeter, and $\pm$ 10 percent for the 20 cm calorimeter. We have used the extrapolation method in interpreting energy data. Thus this calibration verifies our reported energy values.

SECTION 4
COMPARISONS

4.1 IMPULSE DATA.

Figure 12 plots the measured coupling coefficient (I/E) versus fluence E/A) for all cases investigated at MLI. Several techniques were used to measure the impulse; details may be found in Maxwell Report #MLR-2320, "Two-Meter Laser Materials Response Impulse Measurements", April 1986. The data is tabulated in Table 3. Coupling coefficients for the flood-loaded target shots lie well below those for the partially illuminated target, indicating that a significant fraction of the impulse is delivered outside the laser footprint. The coupling coefficient decrease with increasing fluence, with data points ranging from 8.2 dyne·s/J at 330 J/cm^2 to 2.7 dyne·s/J at 1975 J/cm^2. While there is spread between the data from different impulse measurement techniques, the data all show the same trends. All fall above the I/E coefficients found in other experiments except for SPRITE data taken at increased pressures, as can be seen from Figure 13, which shows impulse data from several sources. Experimental conditions and references are listed in Table 4. SPRITE, WRC and MLI show decreasing I/Es with increasing fluence, while the AFWL's LVT data (both at AERL and at MLI) do not.

4.2 PRESSURE DEPENDENCE.

Impulse data have been taken at different pressures. The MLI data were taken over a range of 0.05 to 0.50 torr, with the exception of two Fotonic gauge shots, which were taken at 5 torr. The pressure was noted before each shot, and was checked occasionally after a shot to ensure the fidelity of the pressure measurement. The bulk of the data was not taken over a wide enough range to show any correlation with pressure. The two shots taken at 5 torr do not show an obvious effect on I/E due to pressure. Framing camera pictures taken at MLI, however, do show a definite change in the nature of the plasma plume as the

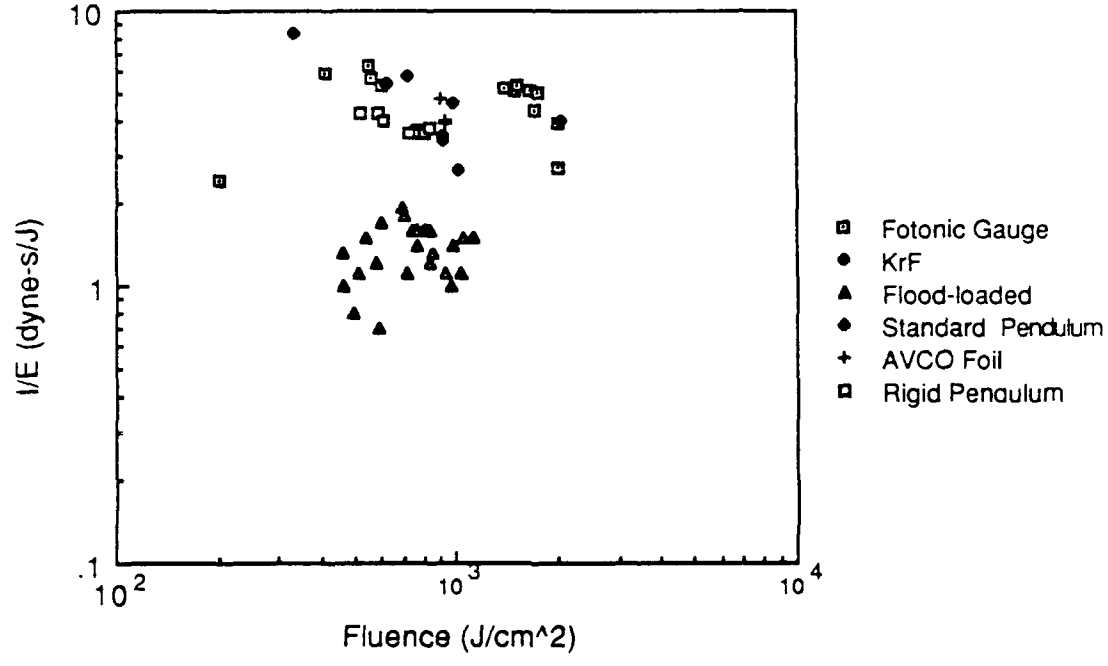

Figure 12. MLI aluminum impulse data.

Table 3. MLI aluminum impulse measurements.

THREAD SUSPENSION

SHOT	I/E (dyne•s/J)	E/A (J/cm^2)
6-14-02	5.8	711
6-14-03	5.4	618
6-14-04	8.2	330
6-14-05	4.6	975
6-14-06	4.0	2038*

* spot size was 1.4 x 2.8 mm^2.

AVCO FOIL

8-23-01	4.0	925
8-23-02	3.9	920
8-23-04	4.8	894

RIGID HANGER

10-29-04	4.2	588
10-30-01	3.7	835
10-30-02	3.6	810
10-30-03	4.0	605
10-30-04	4.2	520
11-05-04	3.6	776
11-05-05	3.6	725

Table 3. MLI aluminum impulse measurements (cont'd).

FLOOD LOAD TARGET

SHOT	I/E (dyne•s/J)	E/A (J/cm^2)
11-01-04	1.6	810
11-07-02	1.5	1120
11-07-03	1.5	1050
01-14-01	1.0	463
01-14-02	1.1	516
01-14-03	0.8	491
01-15-01	1.1	714
01-15-02	0.7	592
01-15-03	1.2	575
01-15-04	1.5	541
01-15-05	1.3	461
01-16-02	1.1	1031
01-16-03	1.2	837
01-16-04	1.0	955
01-16-05	1.1	930
01-16-06	1.4	765
01-16-07	1.6	834
01-17-01	1.3	850
01-17-02	1.4	976
01-17-04	1.7	598
01-17-05	1.6	768
01-17-06	1.8	702
01-17-07	1.6	740
01-17-08	1.9	687

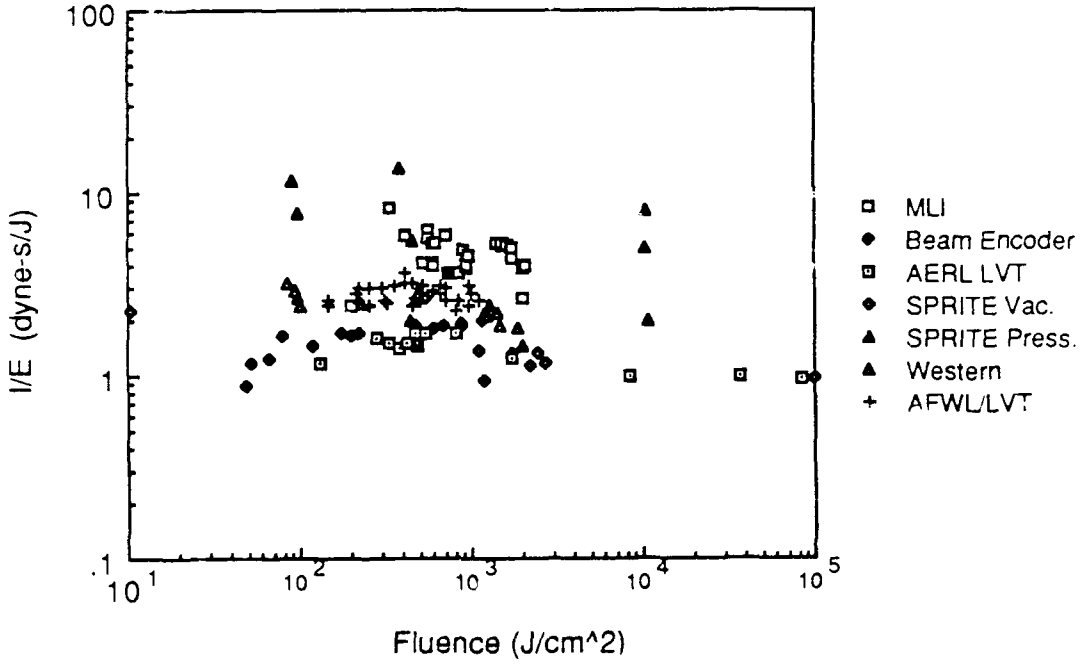

Figure 13. Impulse measurements from several sources.

Table 4. Aluminum experimental parameters.

Location	Wavelength (mm)	Pulselength	Pulseshape	Energy (J)	Fluence J/cm sq	Pressure (torr)	Spot Size (cm sq.)
MLI	351/248	2 μs	square	24-90	200-2,038	.05-5	.036 - .35
AERL	351	1.3 μs	ramped	130-670	48-83,000	0.1-760	.007 - 3.208
SPRITE	248	50 ns	square	67-110	10-146,000	0.01-760	3.5 x 10^-4 - 9.46
WRC	308	.3 -.8 ns	square		85-1,000	0.01	0.008

Location	Reference
MLI	this work, MLR 2320, AFWL-TR-86-155
AERL	AFWL-TR-85-126
SPRITE II	presented by R. Dingus at "Photon Torpedo" Effects Meeting Vol 1 LTH-2 agenda, 9-13 Dec '85 RDA, Marina del Rey
SPRITE III	presented by A.C. Douglas at Lth 2/3 Quarterly Review 10 Dec '86 BDM Conference Site, McLean, VA
WRC	WRC-N-445 (Corrected Data)

pressure is increased from <1 torr to a few torr (See Figure 14 and 15). Researchers at SPRITE found a strong pressure effect; I/E coefficients measured at 760 torr were as much as 10 times higher than those measured at 0.01 torr, other conditions being equal. Work done at AERL, however, showed no pressure dependence, even for atmospheric conditions.

Thus, contradictory results have been found. The SPRITE II and III data support a pressure dependent I/E; the AFWL/AERL data support a pressure independent I/E. Framing camera photographs show a difference in plasma characteristics as the pressure increases from near vacuum to a few torr. This suggests that the interaction is changing over this pressure range; a change in impulse delivery would be expected to occur as well.

4.3 CONCLUSIONS.

MLI has studied impulse generated by laser-target interaction. The impulse was measured using several techniques, and the experimental methods were carefully checked. We find coupling coefficients decline with increasing fluence, lower impulse is measured with a flood-loaded target and I/Es range from ~ 2.5 to 8 d·s/J over fluences ranging from 2000 to 300 J/cm^2.

When the body of data from several researchers is assembled, there are significant differences. These include I/E values for a given fluence, constant vs. varying coupling coefficients for changing fluences, and dependence of impulse on pressure. These unresolved differences indicate that laser generated impulse is sensitive to many different parameters, and that our understanding of their relative importance is incomplete.

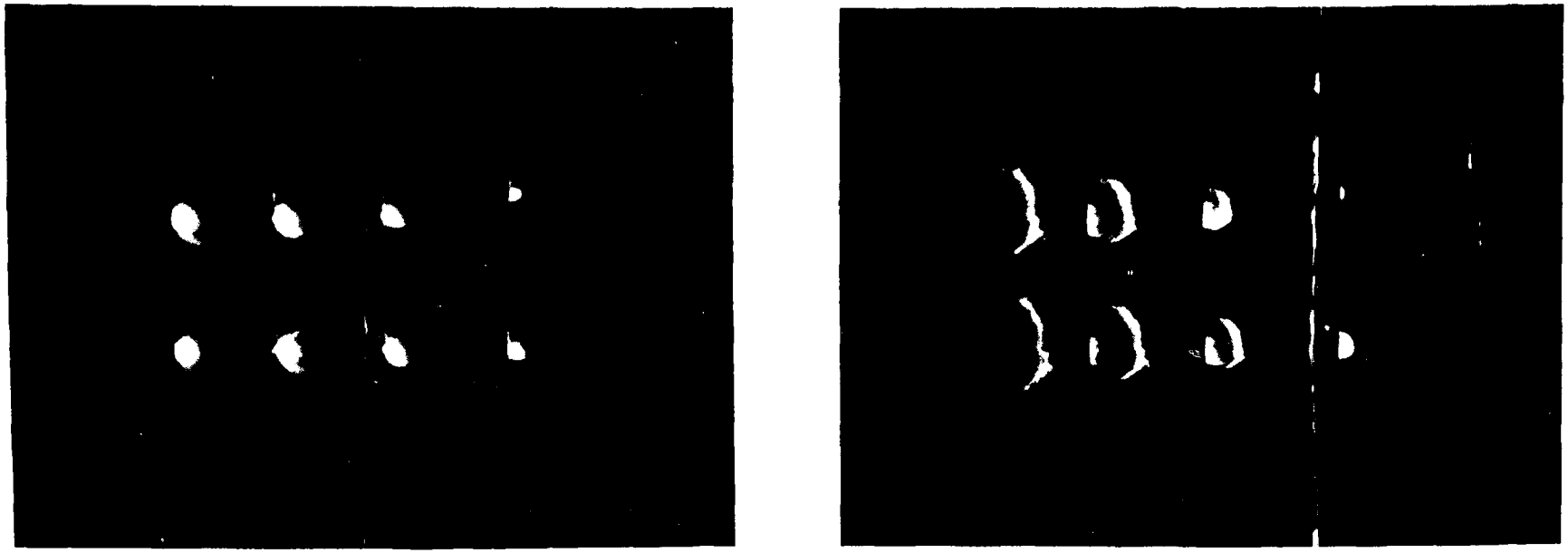

< 1 torr

5 torr

Figure 14. Framing camera pictures of aluminum target plasmas at two chamber pressures. The framing interval is 200 ns and the sequence proceeds in a zigzag pattern from upper right to lower left.

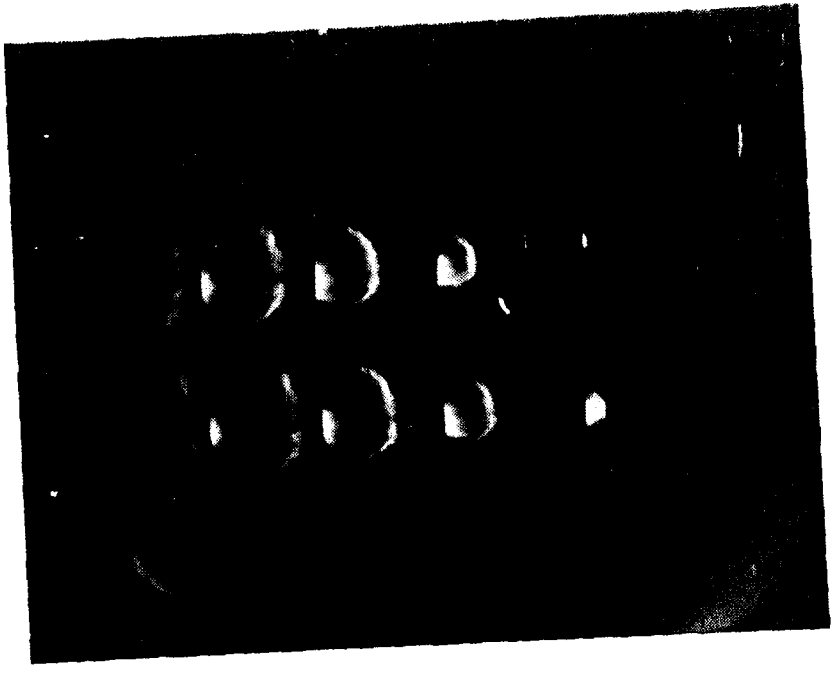

Figure 15. Framing camera picture of aluminum target plasmas at 2.1 torr. The framing interval is 200 ns and the sequence proceeds in a zig zag pattern from upper right to lower left.

DISTRIBUTION LIST

DNA-TR-87-144

DEPARTMENT OF DEFENSE

DEFENSE ADVANCED RSCH PROJ AGENCY
ATTN: F PATTEN

DEFENSE INTELLIGENCE AGENCY
ATTN: RTS-2B

DEFENSE NUCLEAR AGENCY
ATTN: SPWE/MAJ WADE
ATTN: SPSD
4 CYS ATTN: TITL

DEFENSE TECHNICAL INFORMATION CENTER
2 CYS ATTN: DTIC/FDAB

STRATEGIC DEFENSE INITIATIVE ORGANIZATION
ATTN: T/KT LTCOL C MARTIN

DEPARTMENT OF THE ARMY

U S ARMY STRATEGIC DEFENSE COMMAND
ATTN: SDC/E MONTGOMERY

DEPARTMENT OF THE NAVY

NAVAL RESEARCH LABORATORY
ATTN: CODE 4600 D NAGEL

DEPARTMENT OF THE AIR FORCE

FOREIGN TECHNOLOGY DIVISION, AFSC
ATTN: TQX-1, J TUSS

WEAPONS LABORATORY
ATTN: TA/ LT COL W MULZER
ATTN: TA/LT COL HERRERA

DEPARTMENT OF ENERGY

LAWRENCE LIVERMORE NATIONAL LAB
ATTN: F SERDUKE
ATTN: L-84 H KRUGER
ATTN: M GERRISSIMENRO

LOS ALAMOS NATIONAL LABORATORY
ATTN: B259 A GREENE
ATTN: C931 T KING
ATTN: E548 R S DINGUS

SANDIA NATIONAL LABORATORIES
ATTN: DIV 8242 A MCDONALD
2 CYS ATTN: DIV 8242 M BIRNBAUM

SANDIA NATIONAL LABORATORIES
ATTN: DEPT 1230 J POWELL
ATTN: K MATZEN

DEPARTMENT OF DEFENSE CONTRACTORS

APTEK, INC
ATTN: DR S SUTHERLAND

BATTELLE MEMORIAL INSTITUTE
ATTN: C WALTERS

GENERAL RESEARCH CORP
ATTN: W NAUMAN

JAYCOR
ATTN: M TREADAWAY

KAMAN SCIENCES CORP
ATTN: N FERRITER
ATTN: R ALMASSY

KAMAN SCIENCES CORPORATION
ATTN: DASIAC

KAMAN SCIENCES CORPORATION
ATTN: DASIAC

KTECH CORP
ATTN: D KELLER

MCDONNELL DOUGLAS CORPORATION
ATTN: J S KIRBY
ATTN: L THOMPSON

PACIFIC-SIERRA RESEARCH CORP
ATTN: H BRODE

PHYSICAL SCIENCES, INC
ATTN: M MILLER

R & D ASSOCIATES
ATTN: B GOULD
ATTN: D GAKENHEIMER
ATTN: P A MILES

S-CUBED
ATTN: G GURTMAN
2 CYS ATTN: K ROBERTSON
2 CYS ATTN: M CATES

SCIENCE APPLICATIONS INTL CORP
ATTN: E TOTON

SRI INTERNATIONAL
ATTN: B HOLMES
ATTN: D CURRAN
ATTN: G ABRAHAMSON